Thaw Slump Susceptibility Mapping Based on Sample Optimization and Ensemble Learning Techniques in Qinghai-Tibet Railway Corridor

Yi He, *Member, IEEE*, Tianbao Huo, Binghai Gao, Qing Zhu, Long Jin, Jian Chen, Qing Zhang, and Jiapeng Tang

***Abstract*—Thaw slump susceptibility mapping (TSSM) of Qinghai–Tibet railway corridor (QTRC) is the prerequisite and basis for disaster assessment and prevention of permafrost projects. The objective of this article is to construct ensemble learning models based on single classifier models to generate the TSSM of the QTRC, compare and verify the performance of the models, and further explore the relationship between the high susceptibility area and environmental factors of the QTRC. The collinearity analysis was carried out by selecting 14 thaw slump conditioning factors (TSCFs). We used the balance bagging method for sample optimization, and the dataset was divided into 70% training set and 30% verification set. Convolutional neural network, multilayer perceptron, support vector regression, random forest single classifiers were selected to construct blending and stacking ensemble learning models for the TSSM. The results showed that there was no collinearity among the 14 TSCFS. The comparison of model performance revealed that all models had good performance, but the constructed stacking and blending ensemble learning models had stable performance and high prediction accuracy for TSSM. The stacking ensemble learning model had the best effect, and the area under curve value of receiver operating characteristic curve reached 0.9607. It showed that the generated TSSM of QTRC based on stacking ensemble learning model had the highest reliability. The QTRC has local areas with high thaw slump susceptibility, mainly concentrated in the permafrost areas with high altitude, high slope, adjacent faults, sparse vegetation, ice and snow and the more cumulative precipitation.**

***Index Terms*—Ensemble learning, Qinghai–Tibet railway, sample optimization, thaw slump susceptibility mapping (TSSM).**

Manuscript received 3 January 2024; revised 29 January 2024 and 15 February 2024; accepted 18 February 2024. Date of publication 21 February 2024; date of current version 4 March 2024. This work was supported in part by the National Natural Scientific Foundation of China under Grant 42201459, in part by the Key and Development Project of Lanzhou Jiao Tong University under Grant LZJTU-ZDYF2301, and in part by Gansu Science and Technology Program under Grant 23JRRA881. *(Corresponding authors: Binghai Gao; Long Jin.)*

Yi He, Tianbao Huo, Binghai Gao, Long Jin, Jian Chen, Qing Zhang, and Jiapeng Tang are with the Faculty of Geomatics, Lanzhou Jiaotong University, Lanzhou 730700, China, also with the National-Local Joint Engineering Research Center of Technologies and Applications, National Geographic State Monitoring, Lanzhou 730700, China, and also with the Gansu Provincial Engineering Laboratory, National Geographic State Monitoring, Lanzhou 730700, China (e-mail: heyi@mail.lzjtu.cn; 1921412281@qq.com; 1335462199@qq.com).

Qing Zhu is with the School of Earth Science and Environmental Engineering, Southwest Jiaotong University, Chengdu 611756, China.

Digital Object Identifier 10.1109/JSTARS.2024.3368039

I. Introduction

THAW slump is a typical thermal karst landform, which refers to the phenomenon that the underground ice is exposed by natural factors or human activities in the slope area where the underground ice is distributed, so that the melting soil above it loses its support and collapses under the action of its own weight [1], [2]. Thaw slumps that are accompanied by the melting of underground ice will have a series of disaster effects on ecological environment, water environment, climate, and infrastructure [3], [4]. Specifically, thaw slump disasters expose the surface and promote ecosystem degradation [5]; Thaw slump disasters break water balance, releasing chemical solutes and causing water environment pollution [6]; Thaw slump disasters release greenhouse gases and accelerate global warming [7]. In addition, thaw slump disasters will destroy roadbed, block bridges and culverts, and threaten the safe operation of frozen soil projects [8], [9]. In recent years, with the influence of global warming and anthropogenic activities, the number of thaw slumps development has increased rapidly [10], [11]. It is very important to identify the potential thaw slumps. The evaluation of thaw slump susceptibility can predict the probability of potential thaw slumps, which is of great significance for the prevention and control of thaw slump disasters.

The QTRC is a belt area that runs through the south and north. Due to the rapid warming of the global climate, the thaw slump geological hazards in the QTRC show a trend of obvious intensification [12]. In particular, the new thaw slump disasters in recent years not only threaten the safety and stability of existing permafrost projects such as the Qinghai–Tibet railway (QTR), but also have a great impact on the design and operation of future Qinghai–Tibet projects [13]. It is extremely important to carry out comprehensive identification of potential thaw slumps of QTRC. However, there are few reports on the evaluation of thaw slump susceptibility, and even fewer studies on the evaluation of thaw slump susceptibility of the QTRC. Therefore, this article carried out the evaluation of thaw slump susceptibility of QTRC and realized the evaluation of thaw slump susceptibility "one map."

Machine learning methods have the ability to express nonlinear relationships and have been widely explored and applied in susceptibility assessment, such as logistic regression [14], decision tree [15], RF [16], SVM [17], artificial neural

© 2024 The Authors. This work is licensed under a Creative Commons Attribution-NonCommercial-NoDerivatives 4.0 License. For more information, see https://creativecommons.org/licenses/by-nc-nd/4.0/

networks [18], and other neural networks [19], which perform better than general statistical models in susceptibility assessment [20], [21]. In the susceptibility assessment, when facing the classification task of complex scenes, the machine learning methods enhance the more complex nonlinear mapping to generate the end-to-end capability by increasing the layer width and model depth [22]. Accordingly, more sample label data is needed to adapt to the model with larger capacity. Samples in different environments are very different, and it is difficult to ensure the representativeness and balance of samples when samples are selected at random. Unbalanced prediction results will be generated in complex environments, which seriously affects the generalization ability and reliability of machine learning susceptibility evaluation methods. When the sample contains noise, it may even lead to the wrong model being trained [23], [24]. When faced with limited samples, the method of integrating existing models is used to solve this problem. For example, Zhou et al. [25] proposed a landslide susceptibility assessment method based on a coupled model of ensemble learning and radial basis neural network. Wang et al. [26] proposed that the ensemble learning technology of stacking combines CNN and recurrent neural networks to predict landslide hazard vulnerability. Lv et al. [27] proposed a hybrid landslide susceptibility mapping framework based on heterogeneous ensemble learning and deep learning models to evaluate the susceptibility of landslides in the Three Gorges Reservoir area, China. Wu et al. [28] proposed a landslide susceptibility assessment method using Alternating decision tree and a new ensembled technique based on GIS. Di Napoli et al. [29] proposed an ensembled method based on artificial neural network, generalized boosting model and maximum entropy machine learning algorithms to evaluate landslide susceptibility. However, these studies mainly focus on the evaluation of landslide susceptibility, and there are few studies on the evaluation of thaw slump susceptibility. In addition, the blending and stacking ensemble learning methods based on an outstanding deep learning CNN, popular machine learning MLP, SVR, and RF single classifier for TSSM are lacking.

In this article, the QTRC is selected as the research area, and the thaw slump susceptibility is evaluated based on single classifier models and ensemble learning technology. The research objectives are as follows.

1) To optimize thaw slump samples of QTRC based on the balance bagging method.
2) To construct CNN, MLP, SVR, and RF single classifier models to generate the TSSM of QTRC.
3) To construct blending and stacking ensemble learning technology based on CNN, MLP, SVR, and RF single classifier model to generate TSSM.
4) To compare and analyze the performance of single classifier models and ensemble learning models, and verify their accuracy based on InSAR technology.
5) To explore the relationship between the thaw slump high susceptibility area and environmental factors in the QTRC.

The results of this article can provide theoretical and technical support for disaster prevention and control in Qinghai–Tibet project.

II. Study Area and Materials

A. Study Area

The QTR traverses the mid-latitude region of the Qinghai–Tibet Plateau, with a towering terrain with an average altitude of more than 4000 m. The QTR is rich in geological structures and has great differences in topography, landform and regional climate. The permafrost in the QTRC is widely distributed and can be roughly divided into three types of geomorphic units, namely mountain hilly area, fault basin plain area and canyon terrace area. The average annual temperature in the permafrost area is -3.0∼—7.0 °C. Climate warming has a great impact on the geological environment, engineering geological environment and engineering geological conditions of the Qinghai–Tibet railway engineering corridor. Under the background of serious permafrost degradation and global warming on the Qinghai–Tibet plateau, human engineering activities have intensified the permafrost degradation process in the QTRC, and thaw slump disasters have occurred frequently [12], causing certain hidden dangers to railway safety operation. Therefore, it is very important to identify thaw slumps of QTRC in the early stage.

B. Thaw Slumps Database

In this article, we used Google Earth image from October 2022 to February 2023 to visually interpret the thaw slumps of QTRC based on the historical thaw slumps data, and built a thaw slumps database. We identified a total of 707 thaw slumps with a total area of 84.33 km^2 and the largest thaw slump area of 2.88 km^2. The distribution of thaw slumps is shown in Fig. 1.

C. Thaw Slump Conditioning Factors (TSCFs)

Thaw slumps of QTRC were affected by a variety of environmental factors. According to the existing research results and the characteristics of thaw slumps, 14 TSCFs were selected in this article, including altitude, slope, aspect, distance from faults, normalized difference vegetation index (NDVI), land surface temperature (LST), curvature, lithology, frozen soil, distance from QTR, distance from rivers, topographic wetness index (TWI), cumulative precipitation and land use and land cover (LULC). The data details are given in Table I and Fig. 2. To investigate the relationship between thaw slumps and its high susceptibility in detail, we divide the TSCFs into different levels, TSCFS class intervals are given in Table II.

Altitude, slope, aspect, curvature and TWI are calculated by digital elevation model (DEM). distance from faults, distance from QTR and distance from rivers are obtained by euclidean distance interpolation. LST is monthly average temperature that is calculated based on the daily average temperature. Cumulative precipitation is obtained by monthly average precipitation. Finally, all TSCFs are resampled to 30 m spatial resolution.

III. Methodology

In this article, first, the thaw slump samples of QTRC were optimized based on the balanced bagging method, and then the

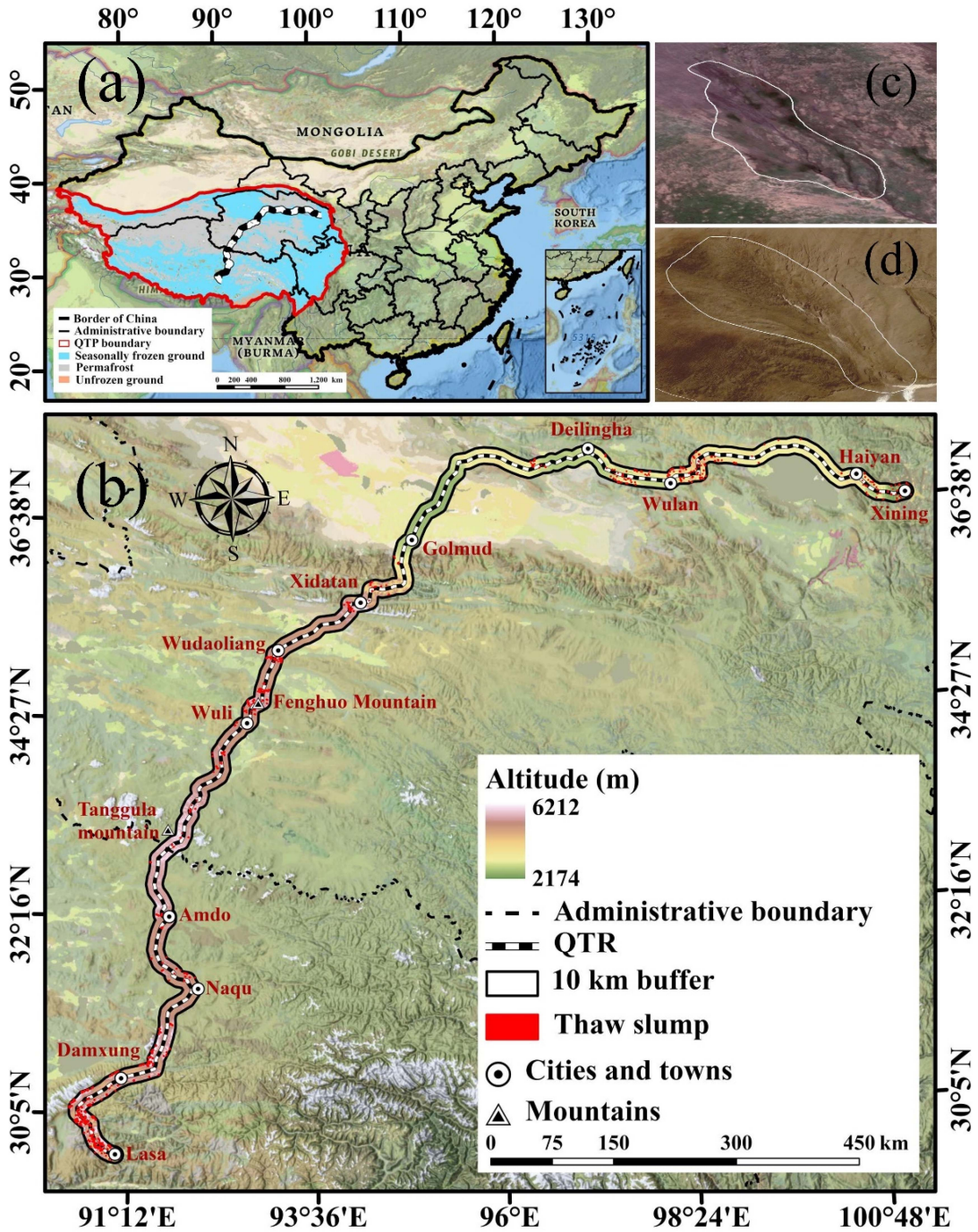

Fig. 1. Overview of the study area. (a) Location of the QTR. (b) Location of the QTRC. (c) (d) Results of our visual interpretation of thaw slumps using Google Earth image.

collinearity of the TSCFs was analyzed based on the collinearity equation. Then, CNN, MLP, SVR and RF single classifier models and blending and stacking ensemble learning technology were constructed, Finally, the performance of the models was compared and analyzed, and TSSMs were generated based on the constructed models. In addition, the results of thaw slump high susceptibility were verified based on InSAR results, and relationship influencing factors and high susceptibility of thaw slumps were discussed. The workflow of this study is shown in Fig. 3.

A. *Sample Optimization Balanced Bagging Method*

Range of QTRC is large and geographical environment is complex, thaw slump samples are imbalance, it is easy to lead to the poor reliability of TSSM, so it is necessary to equalize the thaw slump samples. The balanced bagging classifier is a sample balancing method based on the idea of ensemble learning, which aims to solve the class imbalance problem by redistributing sample weights [31]. In the balanced bagging classifier, each basic classifier is trained by re-weighted samples. These weights

TABLE I
THAW SLUMP CONDITIONING FACTORS DATA

Name	Data sources	Nature of data	Thaw slump factors	Scales/Resolution
DEM	United States Geological Survey (http://earthexplorer.usgs.gov/)	Continuous	Altitude Slope Aspect TWI Curvature	SRTM DEM (30 m)
LULC	Environmental Systems Research Institute (https://www.esri.com/)	Categorical	LULC	Sentinel-2A (10 m)
Precipitation	ERA5-Land (https://cds.climate.copernicus.eu/)	Continuous	Cumulative precipitation	ERA5-Land (1 km)
Vegetation normalization index	National Aeronautics and Space Administration (https://www.earthdata.nasa.gov//)	Continuous	NDVI	MOD13A3 (1 km)
Lithology	International Soil Reference and Information Centre (https://www.isric.org)	Categorical	Lithology	Geological and Lithology Spatial Distribution of China 250 m
Faults	National Earthquake Data Center (https://data.earthquake.cn/)	Categorical	Distance from faults	30 m
Rivers and roads	National Geomatics Center of China (https://www.webmap.cn/)	Categorical	Distance from rivers	Basic Geographical Database of China (30 m)
			Distance from QTR	Basic Geographical Database of China (30 m
Permafrost	Zou et al. [30]	Categorical	Frozen soil	1 km
LST	National Centers for Environmental Information (https://www.ncei.noaa.gov/data/global-summary-of-the-day/archive/)	Continuous	LST	prefecture-level city

are calculated according to the class distribution of the samples, so that the weight of a few samples is higher, and the weight of most samples is lower. In the training process, the basic classifier will pay more attention to the minority class samples, thus improving the classification performance of the minority class, similar to oversampling and under sampling.

Previous studies have shown that SVM model has excellent performance of balancing data samples [32], [33]. In this article, SVM is selected for the base classifier to better find the hyperplane between classification samples. First, the balanced bagging classifier uses bootstrap sampling to resample, and obtains a new training set by sampling from the original training set, thereby increasing the weight of samples of minority classes and improving the learning effect of the classifier on minority classes. Then the weight of the sample is adjusted. Initially, the weight of the sample is initialized according to the class distribution of the sample. The weight of a few class samples is higher, and the weight of most class samples is lower. In the training process, according to the classifier's prediction results and real labels, the misclassified samples are punished, and their

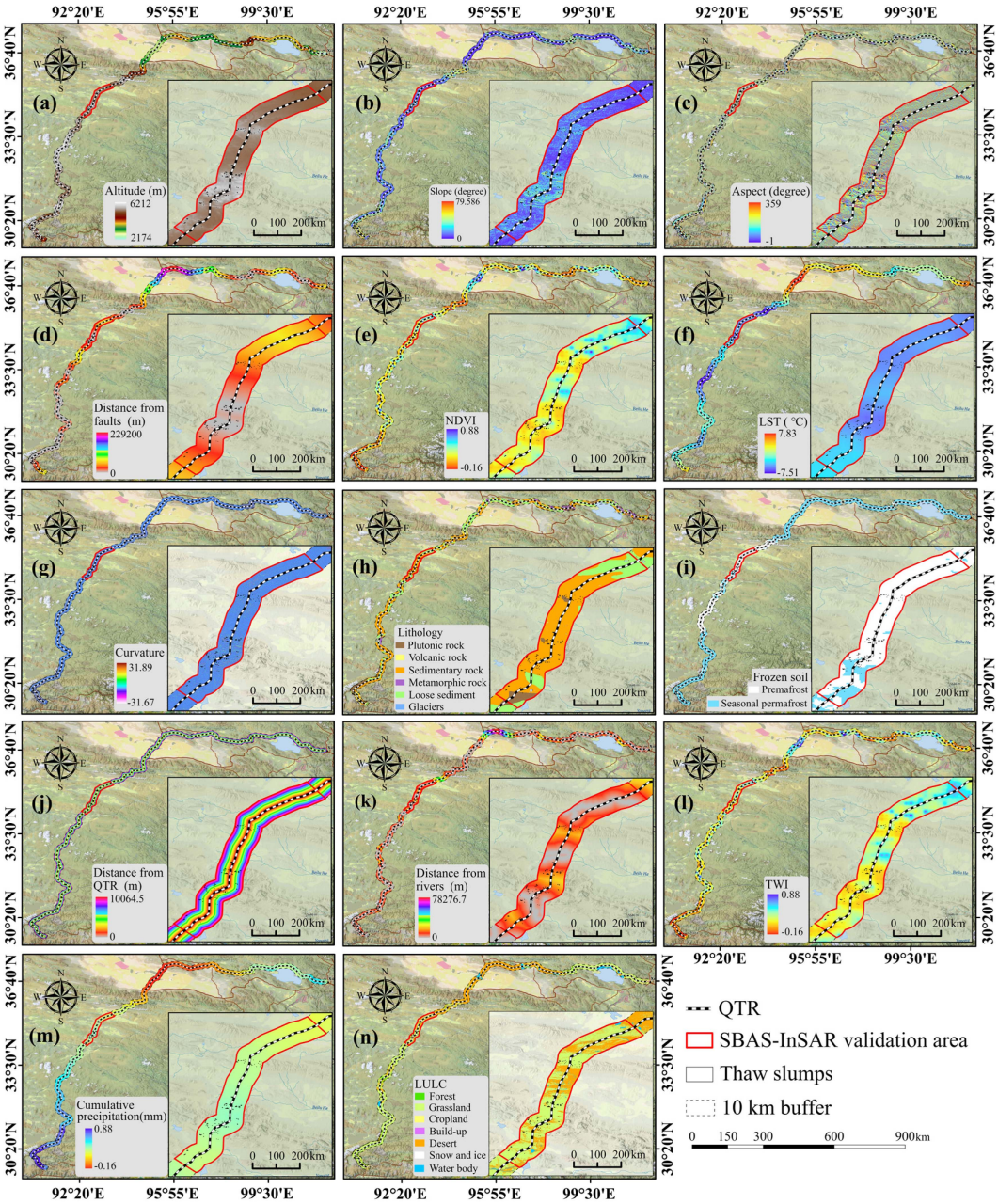

Fig. 2. Spatial distribution of TSCFs. (a) Altitude. (b) Slope. (c) Aspect. (d) Distance from faults. (e) Normalized difference vegetation index. (f) Land surface temperature. (g) Curvature. (h) Lithology. (i) Frozen soil. (j) Distance from QTR. (k) Distance from rivers. (l) TWI. (m) Cumulative precipitation. (n) Land use and land cover.

weights are increased, so that the classifier pays more attention to a few class samples. Finally, the balanced bagging classifier will generate multiple basic classifiers, vote or average the predicted results of all the basic classifiers, and obtain the classification results, thus realizing the problem of unbalanced thaw slump samples of the QTRC. The final equilibrium sample score of this article is 0.8923, and a good sample equalization effect has been achieved. The detailed algorithm is as follows.

B. Machine Learning Models for TSSMs

1) CNN Model: CNN is an excellent method of deep learning. In general, the basic structure of CNN includes a feature extraction layer and a feature mapping layer. In the feature extraction layer, the input of each neuron relates to the local receiving domain of the previous layer, and the local features are extracted [34]. Each computing layer of the network in the feature mapping layer is composed of multiple feature maps. The sigmoid function, which affects the small kernel of the function, is used as the activation function of the convolutional network in the feature mapping structure, which makes the feature maps have displacement invariance. Therefore, CNN is widely used in image recognition and susceptibility assessment [35]. The CNN model consists of five network layers: data input layer; convolution layer; pooling layer; full connection layer; and output layer. In this article, the CNN model is selected as the base

TABLE II
TSCFS AND CLASS INTERVALS

TSCFs	Class	Classified method
Altitude (m)	(1) 2174 to 3034; (2) 3034 to 3538; (3) 3538 to 4176; (4) 4176 to 4694; (5) 4694 to 5023; and (6) 5023 to 6210	Natural break
Slope (°)	(1) 0 to 5; (2) 5 to 9; (3)9 to 16; (4) 16 to 24; (5) 24 to 33; and (6) 33 to 77	Natural break
Aspect	(1) North; (2) northeast; (3) east; (4) southeast; (5) south; (6) southwest; (7) west; and (8) northwest	Equal interval
LST (℃)	(1) -7.5 to -3.9; (2) -3.9 to -1.5; (3) -1.5 to 1.5; (4) 1.5 to 4.6; and (5) 4.6 to 7.9	Natural break
Distance from faults (m)	(1) 0 to 20000; (2) 20000 to 40000; (3) 40000 to 60000; and (4) 60000 to 229201	Equal interval
NDVI	(1) -1 to -0.7; (2) -0.7 to -0.4; (3) -0.4 to -0.1; and (4) -0.1 to 1	Natural break
Curvature	(1) -31 to -0.2; (2) -0.2 to 0.1; (3) 0.1 to 0.3; and (4) 0.3 to 14	Natural break
Lithology	(1) Plutonic rock; (2) volcanic rock; (3) sedimentary rock; (4) metamorphic rock; (5) loose sediment; and (6) glaciers	Lithofacies
Frozen soil	(1) Seasonal permafrost and (2) permafrost	classification
Distance from QTR (m)	(1) 0 to 1000; (2) 1000 to 2000; (3) 2000 to 3000; (4) 3000 to 4000; (5) 4000 to 5000; and (6) >5000	Equal interval
Distance from rivers (m)	(1) 0 to 1000; (2) 1000 to 2000; (3) 2000 to 3000; (4) 3000 to 4000; (5) 4000 to 5000; and (6) >5000	Equal interval
TWI	(1) 5 to 6; (2) 6 to 7; (3) 7 to 8; (4) 8 to 9; (5) 9 to 10; and (6) 10 to 17	Equal interval
Cumulative precipitation (mm)	(1) 0 to 20; (2) 20 to 40; (3) 40 to 60; (4) 60 to 80; (5) 80 to 100; and (6) 100 to 111	Equal interval
LULC	(1) Forest; (2) grassland; (3) cropland; (4) desert; (5) build-up; (6) snow and ice; and (7) water body	Supervised classification

classifier for subsequent ensemble learning, and the structure of the CNN model for the evaluation of thermal thaw slump susceptibility is constructed as shown in Fig. 4. In particular, a 3×3 sized convolutional kernel was used with depths of 32, 48, 64, 96, 128, and 256, respectively. In the model training, batch size was 128, epoch was 120 and the minimum learning rate was 1×10^{-6}.

2) MLP Model: MLP is also called artificial neural network, the hierarchy of MLP is a directed acyclic graph, which can have multiple hidden layers, usually each layer is fully connected to the next layer, the output of each artificial neuron on a layer becomes the input of several artificial neurons in the next layer [36]. MLP can solve nonlinear separable problems and is widely used in susceptibility evaluation [37]. In this article, the MLP model is selected as the base classifier for subsequent ensemble learning, and the structure of the constructed MLP network model is as follows (see Fig. 5), which consists of one input layer, three hidden layers with depths of 512, 256, and 128, respectively, and one output layer The input layer receives the data of TSCFs, the hidden layer learns the features of the TSCFs, and the output layer outputs the prediction result of the thaw slump susceptibility. In the model training, batch size was 128, epoch was 180 and the learning rate was 1×10^{-4}.

3) SVR Model: SVR is an application model for SVM to regression problems, which performs classification and regression tasks by mapping data to a high-dimensional space using kernel functions and by finding an optimal hyperplane in the feature space. SVR has been successfully applied to system identification, nonlinear system prediction and so on, and has achieved good results [38]. SVR creates an interval band on both sides of the linear function (see Fig. 6). No loss is calculated for all samples falling into the interval band, only those outside the interval band are included in the loss function, and then the model is optimized by minimizing the width of the interval band and the total loss. In this article, SVR model is selected as the base classifier for subsequent ensemble learning. Where, the cubic Radial basis function is selected as the kernel function, and the tolerances (TOLs) in the regularization parameters and the insensitive loss function are 1 and 0.1, respectively.

4) RF Model: RF algorithm was first proposed by Breiman [39], which randomly generated multiple decision trees and adopted Bootstrap method for resampling. RF model has the advantages of high algorithm accuracy, can handle large datasets, no need to delete feature variables, can effectively deal with missing data, is not easy to produce overfitting, strong generalization ability and many other advantages, and is widely used in classification, susceptibility assessment and other problems [40]. In this article, RF model is selected as the second-layer high-level classifier of the subsequent integrated model. Among the main parameters, the number of classification trees is 100, the node depth of each tree is 8, and the features of the training sample include the characteristic attributes of the TSCFs.

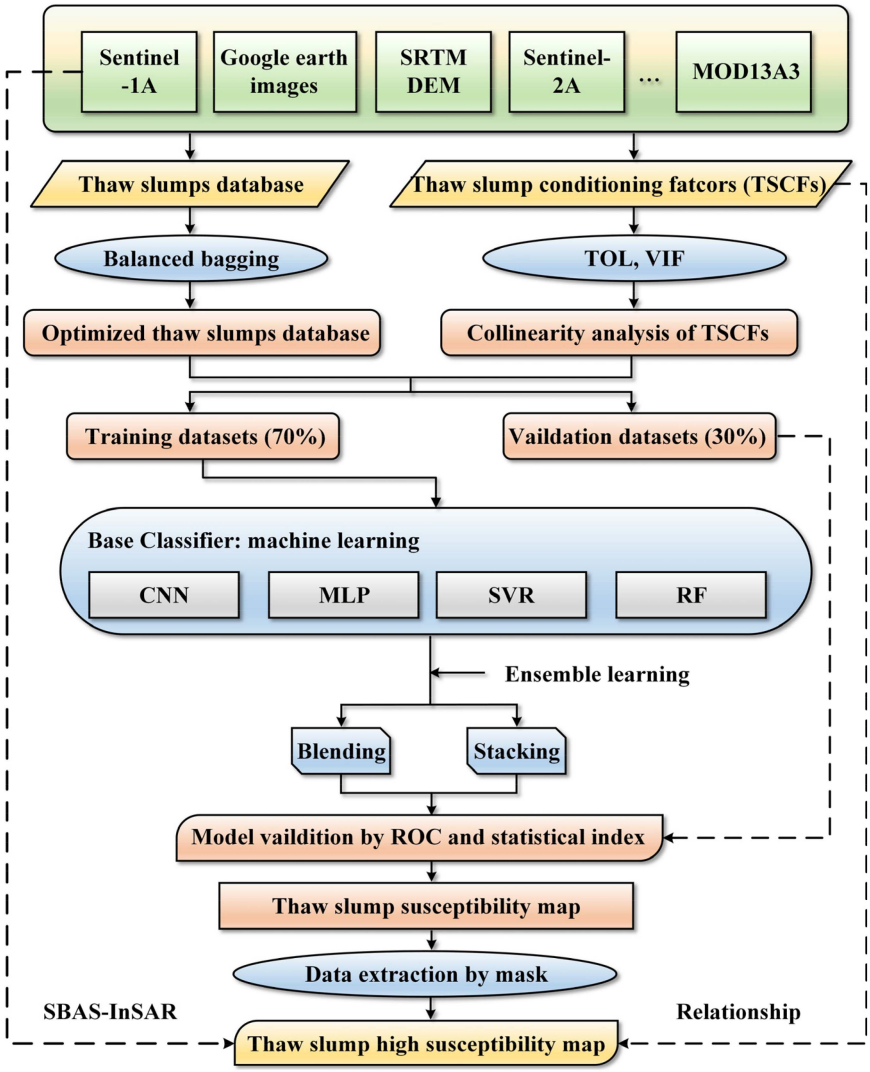

Fig. 3. Schematic diagram of this article.

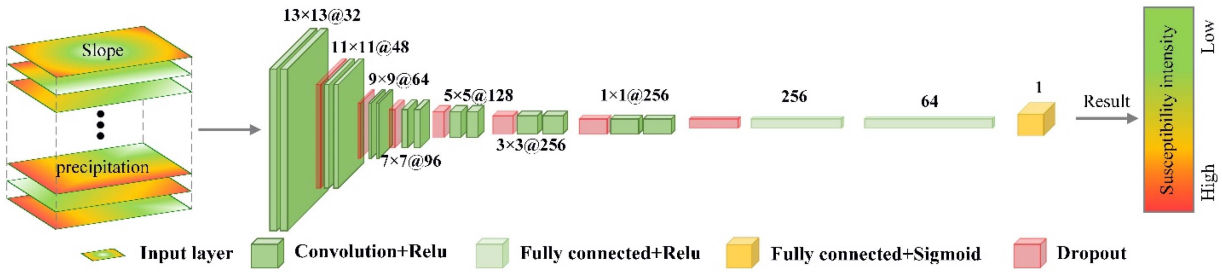

Fig. 4. CNN model for TSSM.

C. Ensemble Learning Models for TSSMs

1) Stacking Ensemble Learning: The stacking method is to stack multiple models (the same layer) in multiple layers to obtain the final stacking results [41]. The stacking method can be understood as the relationship between parallel and series. Generally, models in the first stacking layer use models with a high fit degree to fully learn the training data. The first layer model uses complex nonlinear changes to extract features, and overfitting is easy to occur. Therefore, the second layer model uses simple models, which can complement each other in multiple first-layer models and improve the accuracy and stability of predictions [42]. In this article, CNN, SVR, and MLP are used as the first layer base classifier model, and RF is used as the second layer advanced classifier. The specific framework is shown in Fig. 7.

Algorithm : Actively Balanced Bagging.

Input:

- Training dataset X: The imbalanced thaw slump dataset is divided into training (70%) and test (30%) sets.
- Training labels Y
- Base classifier base_classifier: The base classifier is used SVM method to learn thaw slump features.
- Number of base classifiers n_estimators: The number of estimators is 10.
- Sampling ratio ratio: The ratio is 1.0.
- Balancing method balancing_method: Balancing method is a strategy or method used to balance the dataset during the training process. In this study, under sampling method is used to randomly remove samples from the majority category to equal the number of the minority category.

Output:

- Ensemble classifier ensemble_classifier

Procedure:

1. Initialize an empty ensemble classifier ensemble_classifier
2. For each index i of the base classifier in {1, 2, …, n estimators}, do the following:
   - 2.1 Extract a balanced subset X_balanced, Y_balanced from the training dataset using the balancing method balancing_method
   - 2.2 Randomly sample a training subset X_train, Y_train from X_balanced, Y_balanced using the ratio ratio
   - 2.3 Fit the base classifier base_classifier on the training subset X_train, Y_train
   - 2.4 Add the base classifier to the ensemble classifier ensemble_classifier
3. Return ensemble_classifier

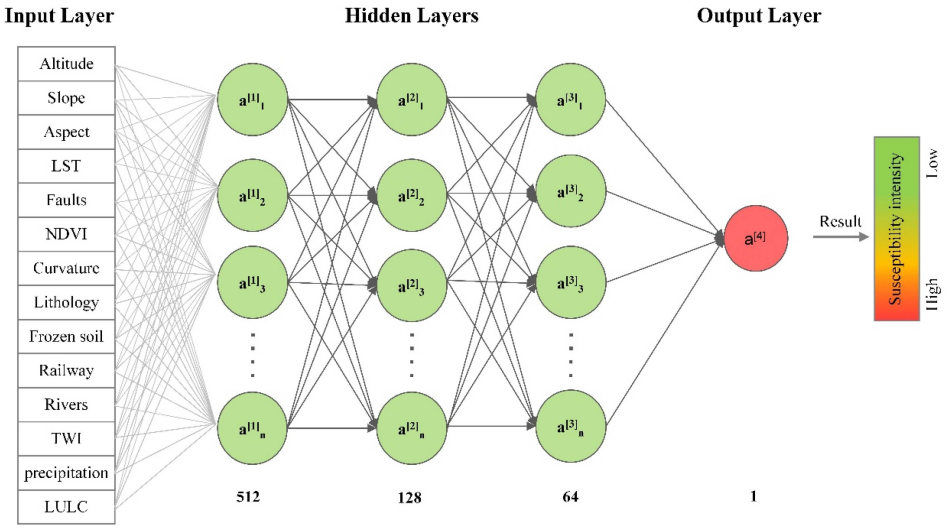

Fig. 5. MLP network model for TSSM.

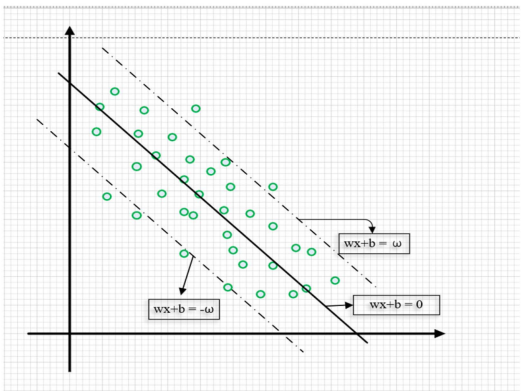

Fig. 6. SVR model.

2) Blending Ensemble Learning: Blending is another form of ensemble learning technique that is derived from stacking [43], the only difference between the two models is that the blending model uses a retained (verified) set from a training set to make predictions. Simply put, predictions are made only for the retained dataset, and the retained dataset and predictions are used to build the second-level model. The specific operation process is as follows: the training data is divided, a part of the divided training data is trained on the base model, and other part is predicted by the model as a new feature training meta-model. The test data is also predicted by the base model to form new test data. Finally, the metamodel makes predictions about the new test data. The specific framework is shown in Fig. 8.

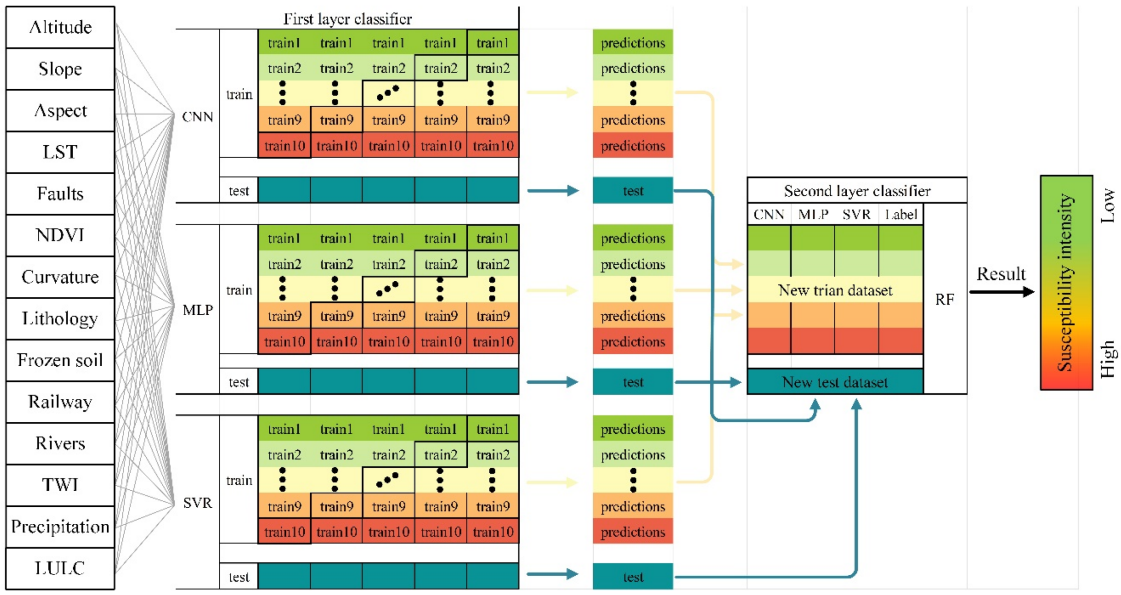

Fig. 7. Stacking ensemble learning model for TSSM.

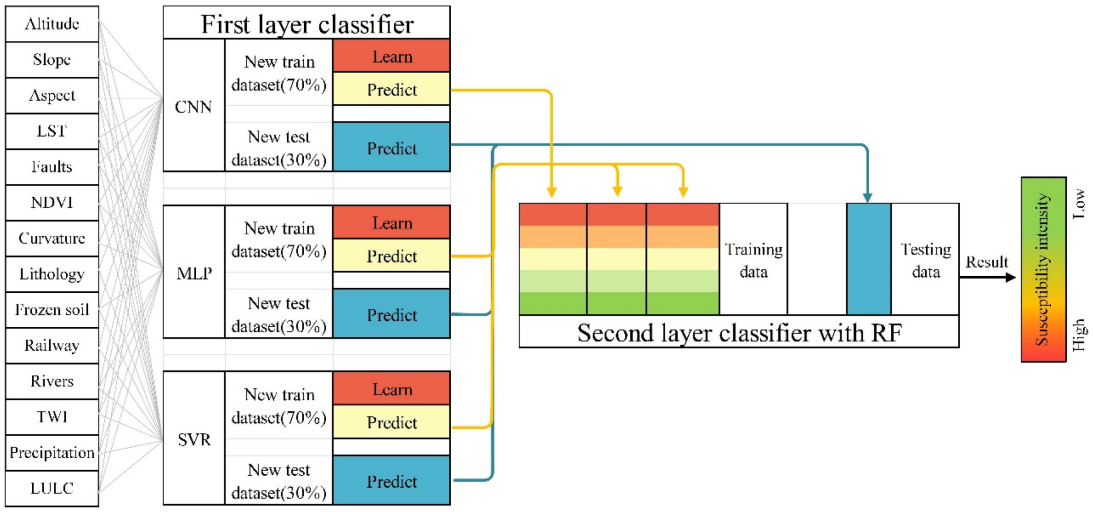

Fig. 8. Blending ensemble learning model for TSSM.

D. Model Evaluation

In this article, eight statistical indicators were selected to evaluate the models, including accuracy, G-mean, specificity, recall, precision, Heidke skill score (HSS), Matthew correlation coefficient (MCC), and Kappa. In addition, ROC curve was also selected to evaluate the performance of the prediction model [44], [45]. The detailed description of various indicators is shown in Fig. 9.

IV. Results

A. Multicollinearity Analysis of TSCFs in QTRC

Multicollinearity refers to the fact that the model estimation is distorted or difficult to estimate accurately due to the existence of exact correlation or high correlation between explanatory variables in the linear regression model [46]. Therefore, it is necessary to carry out multicollinearity analysis of TSCFs in QTRC. Variance inflation factor (VIF) and TOL are used in this article to analyze the collinearity of TSCFs [47]. VIF is less than 10 and TOL is greater than 0.1, indicating that there is no collinearity problem among the TSCFs, and it can be used for model training [37]. In this article, the VIF and TOL values among the selected TSCFs were calculated, and the results were shown in the Fig. 10. As can be seen from the Fig. 10, the VIF value of the thaw slump impact factor LST was the largest, which was 7.340, and the VIF value of curvature was the smallest, which was 1.094. The VIF value of all the selected TSCFs was less than 10. The TOL values of all TSCFs were greater than 0.1, among which the TOL value of curvature was the largest (0.914) and that of LST was the smallest (0.136). It showed that there was no collinearity among the selected TSCFs in QTRC in

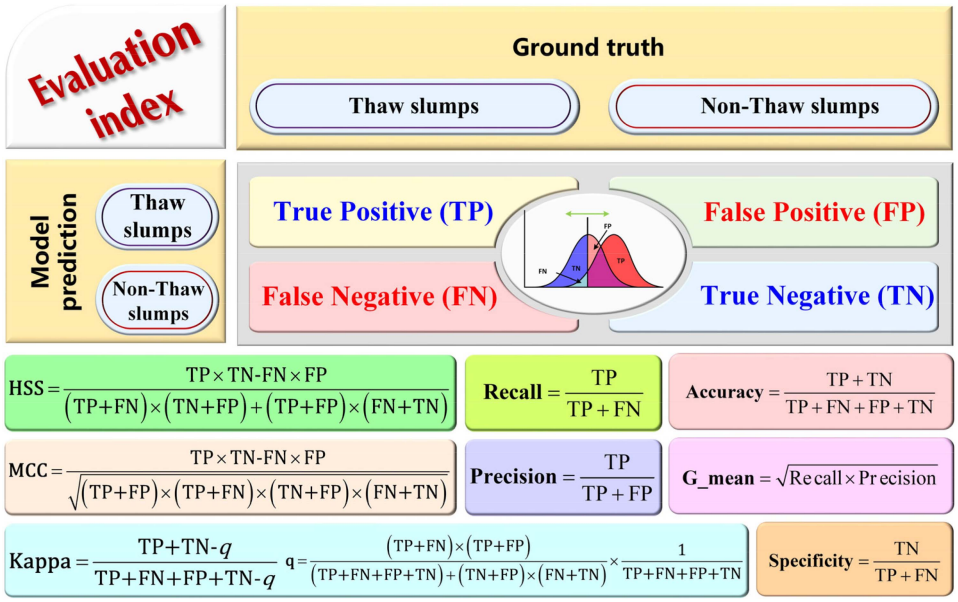

Fig. 9. Confusion matrix and evaluation index.

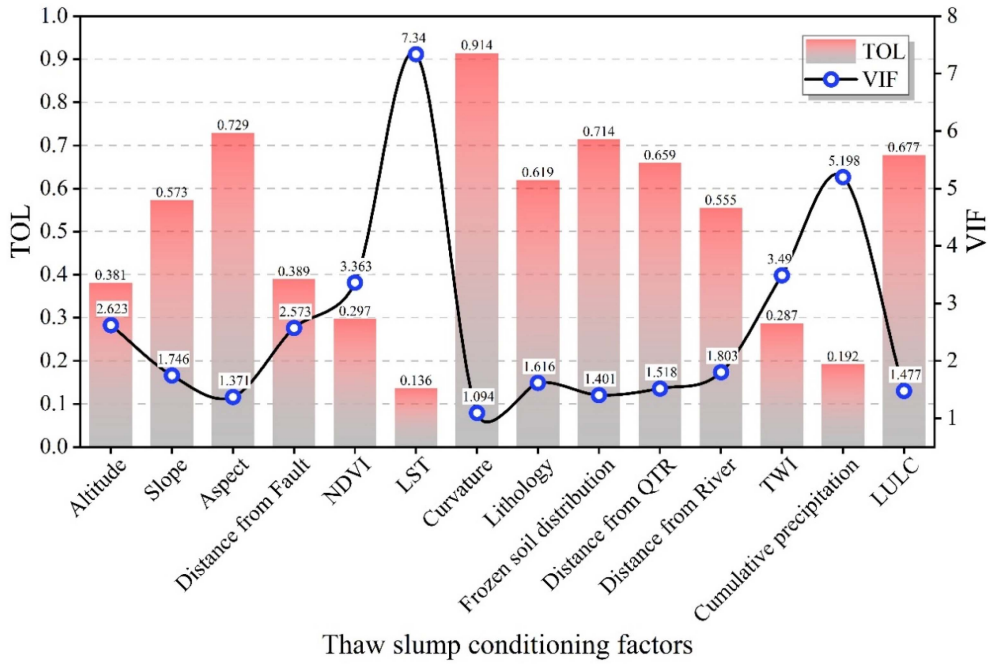

Fig. 10. Collinearity analysis of TSCFs in QTRC.

this article, and the TSCFs are independent of each other, which will not be distorted in the subsequent model training and can accurately predict the thaw slump susceptibility [35].

B. Accuracy and Performance Analysis of the Models

The verification dataset is not used to train the model, so the verification dataset is applied to evaluate the accuracy and performance of the model, we calculated various evaluation indicators, and the results are shown in Fig. 11. Specificity represents the percentage of correct classifications in all categories of a negative sample; Kappa coefficient measures the classification accuracy; Recall represents the proportion of positive samples with correct prediction; G-mean is a system performance evaluation index for specificity and recall. Precision represents the proportion of predicted positive samples in the predicted positive samples; MCC is a comprehensive evaluation index; Accuracy measures how many samples are correctly identified in the two categories; HSS is a measure of correct prediction ability. The calculation results of these indicators are much greater than 0.5 in six models, which shows that all the evaluation models of thaw slump susceptibility have good prediction ability, and the

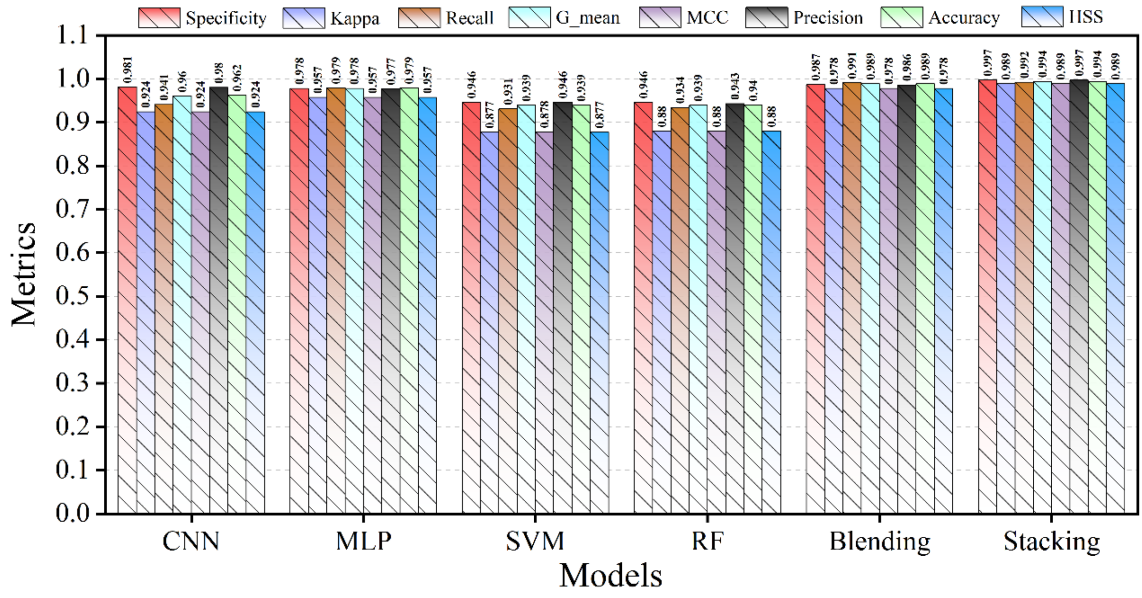

Fig. 11. Statistics of multiple indicators for six models.

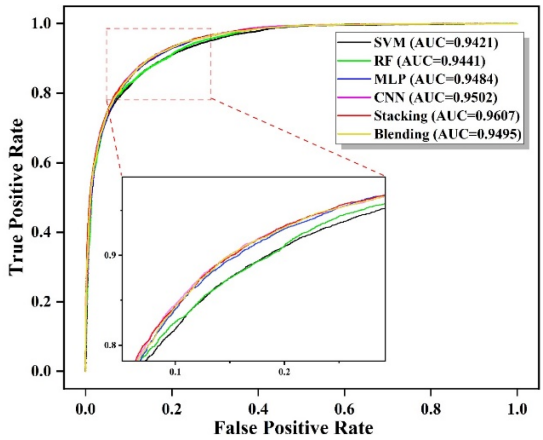

Fig. 12. ROC curve of thaw slump susceptibility prediction model.

predicted TSSM of QTRC is reliable. However, the statistical values of all indicators of the constructed stacking ensemble learning model are the highest, followed by the blending model, and the values of the SVR and RF models are the lowest, revealing that the constructed ensemble learning model mining the advantages of a single weak classifier, enhancing features, and improving the reliability of TSSM.

ROC curve has been widely used in geological hazard model evaluation [48]. AUC is the area under the ROC curve, and the larger the area, the better the model performance [49]. Therefore, AUC was used to reveal the total performance of the thaw slump susceptibility models. The AUC value was calculated based on validation dataset in this article and the results were shown in Fig 12. The AUC values of all models were more than 0.94, indicating all models have good performance. The AUC value of the constructed stacking ensemble learning model was the highest, reaching 0.9607, followed by the constructed blending ensemble learning model, and the AUC value of the SVR model is the lowest, reaching 0.9421. Based on the outcome, the constructed ensemble learning models had the best prediction performance and the most stable, especially the constructed stacking ensemble learning model has better accuracy, TSSM is more reliable than that of the other models.

C. *Thaw Slump Susceptibility Mapping (TSSM)*

In this article, based on the CNN, MLP, SVR, RF single classifier and constructed blending, stacking ensemble learning methods, the TSSMs were generated, and the natural breakpoint statistical method was used to divide it into very high (VH), high (H), medium (M), low (L), and very low (VL) susceptibility. The results were shown in Fig. 13. Based on the six types of thaw slump susceptibility plots of CNN, MLP, SVR, RF, constructed blending and stacking models, the distribution of TSSMs was similar, but the range of high susceptibility areas predicted by SVR model was larger. Thaw slumps were mostly distributed in the high susceptibility areas.

We have calculated the distribution proportions of each level of thaw slump susceptibility in the QTRC generated by six models, and the results are shown in Fig. 14. The proportion of very high and high susceptibility areas predicted by CNN, MLP, SVR, RF, constructed blending and stacking models were 12.11%, 13.76%, 15.12%, 14.11%, 13.11%, and 13.78%, respectively. The high susceptibility areas predicted by the CNN, MLP, SVR, RF, constructed blending and stacking models accounted for 85.62%, 86.35%, 86.29%, 85.17%, 85.30%, and 86.12% of all thaw slumps, respectively. It can be observed in all models that 85% of the thaw slumps is distributed in the high susceptibility areas, indicating that the six models have good prediction results.

Based on the above analysis, the TSSM obtained by the proposed stacking ensemble learning model has the highest precision. Therefore, we select the TSSM result to analyze the thaw slump characteristic of QTRC. Due to the large area of

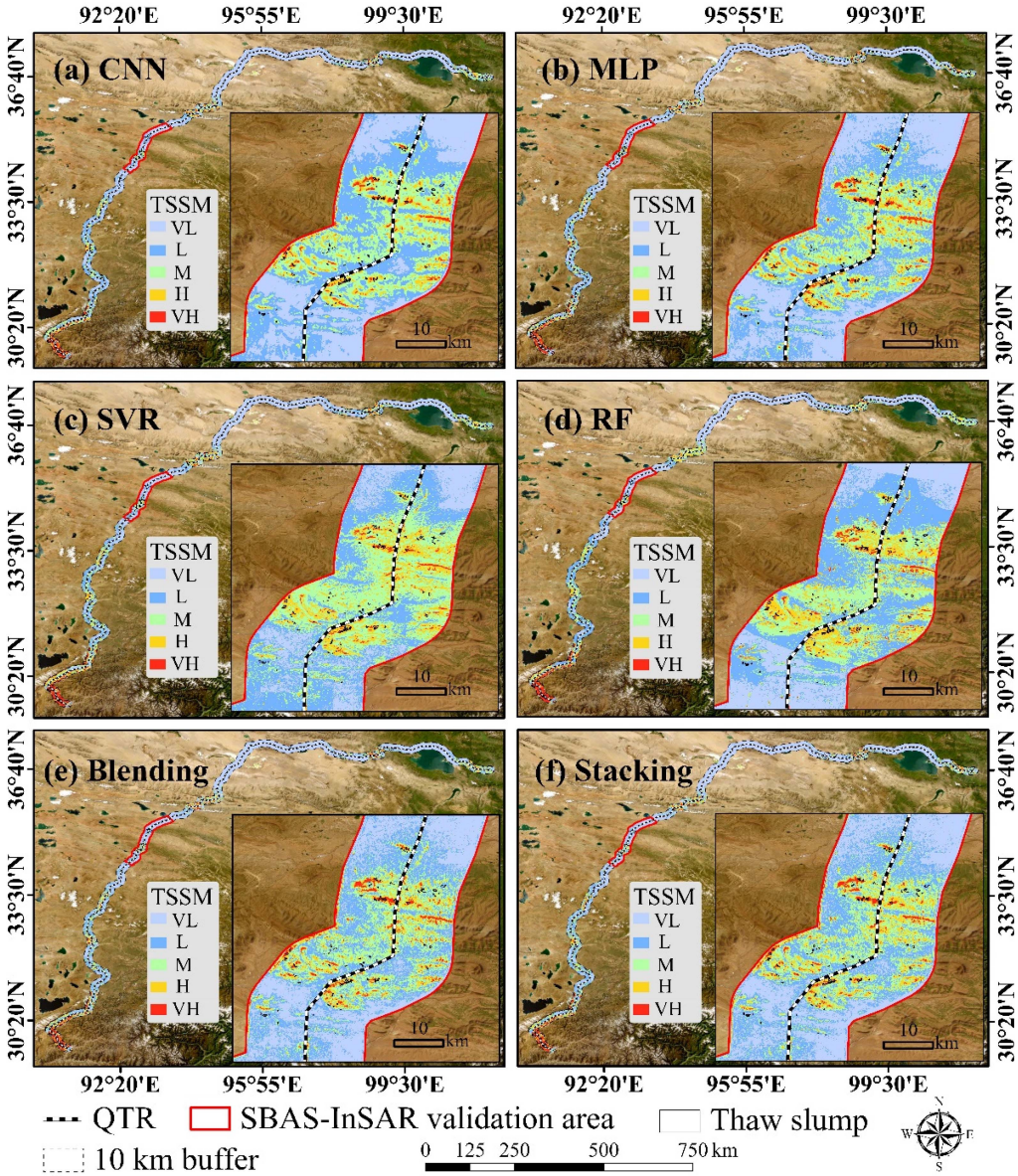

Fig. 13. Distribution of TSSMs based on CNN (a) multilayer perceptron, (b) support vector regression, (c) random forest, (d) constructed blending, (e) stacking ensemble learning, and (f) models.

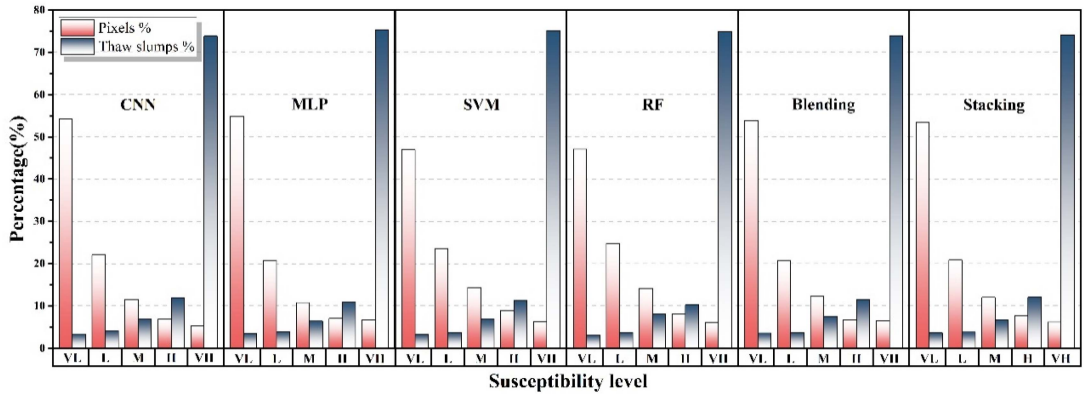

Fig. 14. Proportion of each level of thaw slump susceptibility predicted by the six models and the distribution of thaw slumps.

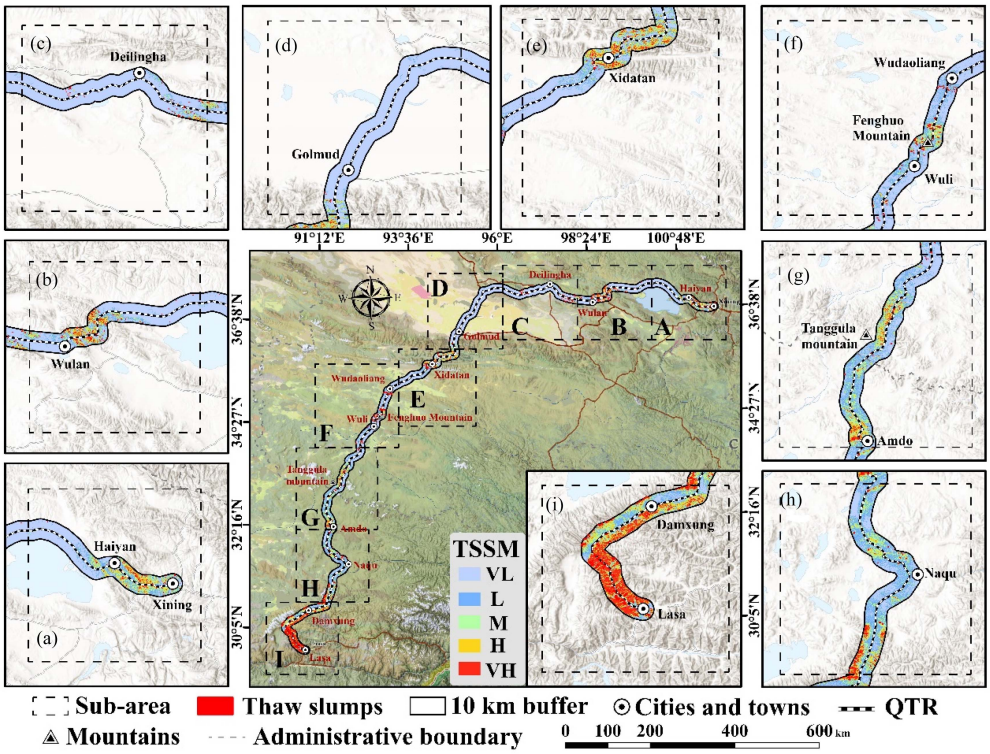

Fig. 15. Distribution of TSSMs based on CNN, MLP, SVR, RF, constructed blending and stacking ensemble learning models. (a)∼(i) are 9 consecutive areas along the QTR.

the QTRC, we divided it into nine areas for visual display (see Fig 15). The thaw slump susceptibility area of QTRC showed local differences, and there were more high thaw slump susceptibility areas in the western section (G, H, and I areas). At the same time, some high and very high-risk areas are predicted on both sides of the QTR. These areas belong to potential risk areas and are very likely to occur thaw slumps in the future, which should be paid attention to.

V. Discussion

A. Evaluation of the Ensemble Learning Models

Accurate and reliable susceptibility maps are crucial in disaster management [23], [49], [50]. In recent years, machine learning single classifiers and ensemble learning have been widely used in susceptibility assessment [42], [51], [52]. The objective of this article is to construct the blending and stacking ensemble learning methods for TSSM based on CNN, MLP, SVR, and RF single classifiers. CNN is an outstanding deep learning models for susceptibility mapping [34], MLP, SVR, and RF are popular machine learning model for susceptibility mapping [37], [38], [39], CNN, MLP, SVR, and RF are selected as base classifiers, and it is bound to get better susceptibility mapping results when constructing ensemble learning models. Among them, CNN, MLP, and SVR are used as the first classifier and RF is used as the second classifier. Generally, in ensemble learning models, the first layer model fully learns complex nonlinear changes to extract features of the training data, and the second layer model complement each other in multiple first-layer models and improve the accuracy and stability of predictions [42]. Therefore, the first layer model is relatively complex, the second layer model is relatively simple. The constructed ensemble learning in this article meets this requirement. Therefore, the ensemble learning model we constructed is reasonably structured. All statistical index values also show that the constructed ensemble learning model is the highest, which further proves that the constructed ensemble learning model in this article is reliable.

Ensemble learning performs better than single classifier, because ensemble learning usually integrates multiple single classifiers, so that they can complete the learning task together, multiple classifiers can help each other, take advantage of each other, and the learning task is more beautiful [42]. Our research results show that the constructed ensemble learning performance is better than that of the single classifier. The results of this article are also consistent with previous studies, ensemble learning can improve the performance of single classifiers and obtain better results of susceptibility mapping [25], [26], [42]. Therefore, the evaluation results of thaw slump susceptibility generated by the constructed ensemble learning model are reliable in the QTRC.

B. InSAR Verification of TSSM Based on Stacking Ensemble Learning Model

Based on the CNN, MLP, SVR, RF single classifier and blending, stacking ensemble learning methods, we have evaluated the thaw slump susceptibility of QTRC. Through the analysis of the results, it is found that the stacking ensemble learning model has the highest reliability. To further verify the prediction accuracy

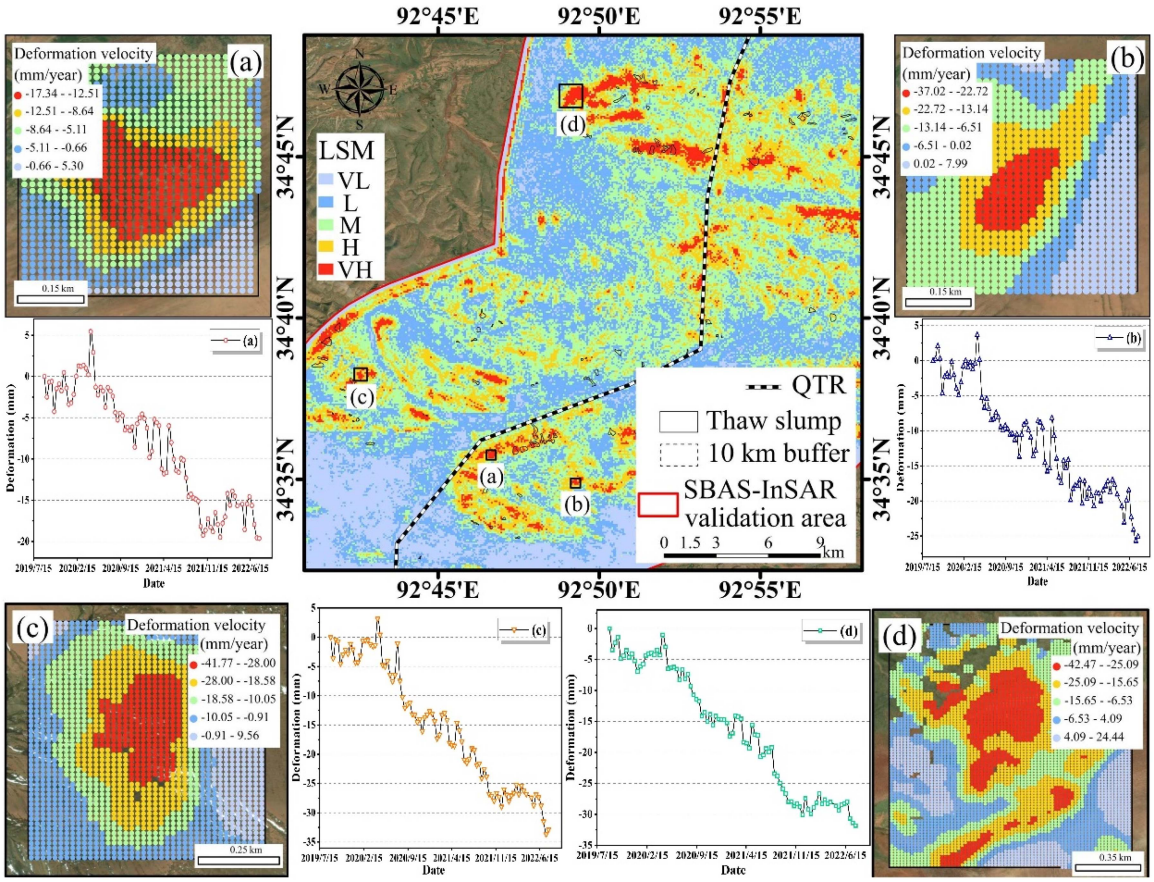

Fig. 16. InSAR verification of thaw slump high susceptibility of QTRC. (a)–(d) Are four TSSM validation regions.

of thaw slump susceptibility, we conduct validation based on interferometric synthetic aperture radar (InSAR) deformation results. InSAR technology is widely applied to monitor the slow deformation of landslides, land subsidence and other disasters [53], [54], [55], [56]. If there is the deformation in InSAR results in the high susceptibility areas predicted by our proposed model, the reliability of our predicted results can be reflected.

Typical areas in the permafrost region of QTRC are selected, and the stacking prediction results with the best performance were used for InSAR verification. In this article, we use SBAS-InSAR technology [57] to obtain the surface deformation of the typical frozen soil region from 2019 to 2022 and select the typical thaw slumps for verification. Where the surface deformation data is based on the SARscape 5.6.2 software of Environment for Visualizing Images platform, the multilook, max normal baseline (%), max temporal baseline (days) and coherence threshold are set to 4:1, 10, 90, and 0.25, respectively. The filtering method, unwrapping method and atmospheric correction method are used Goldstein adaptive filtering algorithm, minimum cost flow algorithm and generic atmospheric correction online service. The verification results are shown in the following Fig. 16. The cumulative surface deformation of typical regions a, b, c, and d were increasing continuously, and the deformation rate of the thaw slumps surface is large. These typical regions are all located in the predicted high-susceptibility areas. This suggests that InSAR deformation exists in the high susceptibility predicted area of thaw slumps. Therefore, the prediction results of thaw slump susceptibility in this article can be proved to be credible.

C. Analysis of Influencing Factors of Thaw Slump High Susceptibility in QTRC

From the above analysis, the TSSM generated by stacking ensemble learning has the highest reliability. We select the high susceptibility areas generated by stacking ensemble learning to explore the relationship between high susceptibility areas and the influencing factors of thaw slumps. We count the number of factors pixels of 14 thaw slump influencing factors and the frequency ratio (FR) value of high susceptibility areas in each level, and the results are shown in the Fig. 17. The proportions of high susceptibility pixels of thaw slumps are high at high altitude in the QTRC, indicating that thaw slumps are easy to develop at high altitude. The proportions of high susceptibility pixels of thaw slumps are high with slope greater than 10°. The proportions of high susceptibility pixels of thaw slumps are high in north and west direction. The closer the distance from faults are, the higher the proportions of high susceptibility pixels of thaw slumps. The lower the NDVI value, the higher the proportions of high susceptibility pixels of thaw slumps. The proportions of high susceptibility pixels of thaw slumps are the highest with LST between -1.5°C and 1.5°C. The proportions of high susceptibility pixels of thaw slumps are high in acid

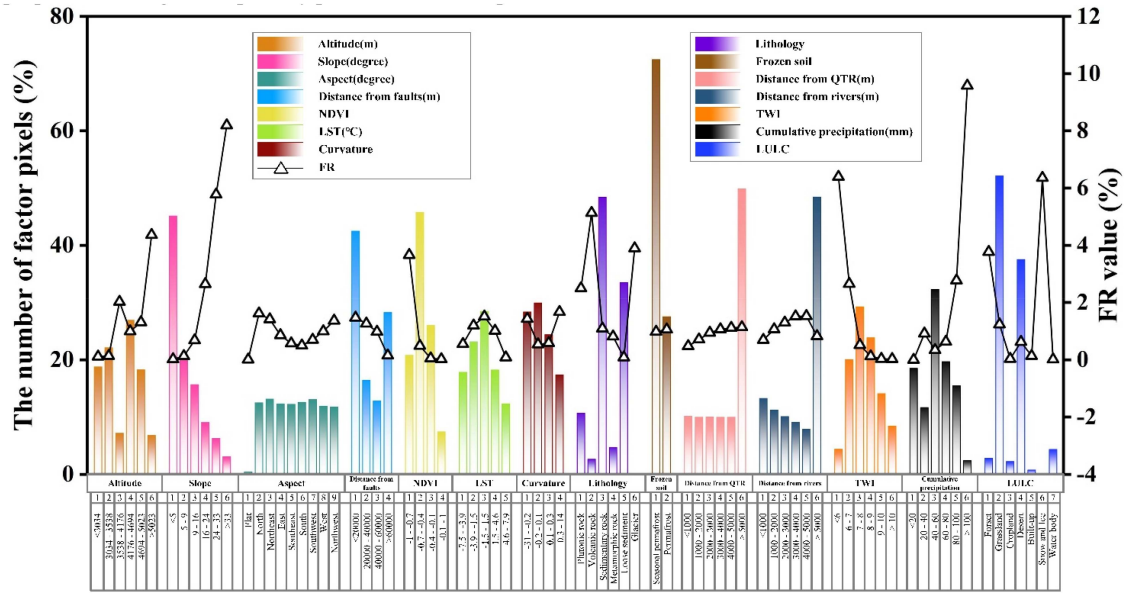

Fig. 17. Relationship influencing factors and high susceptibility of thaw slumps.

volcanic and ice and glaciers lithology. The father the distance from QTR is, the higher the proportions of high susceptibility pixels of thaw slumps. The proportions of high susceptibility pixels of thaw slumps are the highest with distance from rivers between 3000 and 5000 m. The lower the TWI value, the higher the proportions of high susceptibility pixels of thaw slumps. The more the cumulative precipitation, the higher the proportions of high susceptibility pixels of thaw slumps. The proportions of high susceptibility pixels of thaw slumps are high in snow and ice regions.

According to analysis of thaw slump high susceptibility results obtained by experiments, the thaw slumps in the QTRC are mainly distributed in areas with high altitude, high slope, adjacent faults, sparse vegetation, ice, and snow regions and the more cumulative precipitation. These conclusions are also in good agreement with the formation mechanism of thaw slumps [1], [2], which further indicates that the TSSM generated by the models constructed in this article is reliable and credible.

VI. Conclusion

In recent years, with the influence of global warming and anthropogenic activities, the number of thaw slumps development has increased rapidly in the QTRC. It is very important to predict the probability of potential thaw slumps. In this article, we generate the TSSM of QTRC. First, we optimized thaw slump samples of QTRC based on the balance bagging method and analyzed the collinearity among the 14 TSCFS. Then, blending and stacking ensemble learning models were constructed for the TSSM based on CNN, MLP, SVR, and RF single classifiers. Finally, the performance of CNN, MLP, SVR, and RF single classifier models and the constructed blending and stacking ensemble learning models were evaluated by ROC and statistical indexes. This article results showed that the final equilibrium sample score of this article is 0.8923, and a good sample equalization effect had been achieved. There was no collinearity among the selected 14 TSCFS. The constructed stacking and blending ensemble learning models had stable performance and high prediction accuracy for TSSM. The stacking ensemble learning model had the best effect, and AUC value reached 0.9607, the generated TSSM of QTRC had the highest reliability. The QTRC has local areas with high susceptibility of thaw slumps, mainly concentrated in the permafrost areas.

This article generated TSSMs based on sample optimization and ensemble learning techniques. It provided data and technical support for disaster reduction and prevention in Qinghai–Tibet railway corridor. We used the balanced bagging method to optimize the samples, however, the balance of samples was not considered in a similar pregnancy disaster environment, resulting in a high false alarm rate of the TSSM results. In future studies, we will select samples based on the constraints of similar pregnancy-disaster environments to ensure the balance of positive and negative samples in similar pregnancy-disaster environments. In addition, the existing susceptibility assessment models lack learning across spatial environment features, leading to insufficient reliability of prediction results. In the future, we will conduct the susceptibility assessment models based on graph networks.

References

[1] I. Nitze, G. Grosse, B. M. Jones, V. E. Romanovsky, and J. Boike, "Remote sensing quantifies widespread abundance of permafrost region disturbances across the Arctic and Subarctic," *Nature Commun.*, vol. 9, no. 1, 2018, Art. no. 5423.

[2] J. Luo, F. Niu, Z. Lin, M. Liu, G. Yin, and Z. Gao, "The characteristics and patterns of retrogressive thaw slumps developed in permafrost region of the Qinghai-Tibet Plateau," *J. Glaciol. Geocryol.*, vol. 44, no. 1, pp. 96–105, 2022.

[3] P. F. Schuster et al., "Permafrost stores a globally significant amount of mercury," *Geophys. Res. Lett.*, vol. 45, no. 3, pp. 1463–1471, 2018.

[4] M. M. Yao, Z. J. Lin, X. W. Fan, A. Y. Lan, and W. J. Li, "Development characteristics and disaster effects of thaw slump in Hoh Xil, in the hinterland of Qinghai-Tibet Plateau," *J. Glaciol. Geocryol.*, vol. 45, no. 4, pp. 1242–1253, 2023.

[5] S. V. Kokelj and M. Jorgenson, "Advances in thermokarst research," *Permafrost Periglacial Processes*, vol. 24, no. 2, pp. 108–119, 2013.

[6] K. A. St. Pierre, S. Zolkos, S. Shakil, S. E. Tank, V. L. St. Louis, and S. V. Kokelj, "Unprecedented increases in total and methyl mercury concentrations downstream of retrogressive thaw slumps in the western Canadian Arctic," *Environ. Sci. Technol.*, vol. 52, no. 24, pp. 14099–14109, 2018.

[7] M. R. Turetsky et al., "Carbon release through abrupt permafrost thaw," *Nature Geosci.*, vol. 13, no. 2, pp. 138–143, 2020.

[8] Q. Wu, Y. Sheng, Q. Yu, J. Chen, and W. Ma, "Engineering in the rugged permafrost terrain on the roof of the world under a warming climate," *Permafrost Periglacial Processes*, vol. 31, no. 3, pp. 417–428, 2020.

[9] J. Hjort, D. Streletskiy, G. Doré, Q. Wu, K. Bjella, and M. Luoto, "Impacts of permafrost degradation on infrastructure," *Nature Rev. Earth Environ.*, vol. 3, no. 1, pp. 24–38, 2022.

[10] A. G. Lewkowicz and R. G. Way, "Extremes of summer climate trigger thousands of thermokarst landslides in a High Arctic environment," *Nature Commun.*, vol. 10, no. 1, 2019, Art. no. 1329.

[11] A. Runge, I. Nitze, and G. Grosse, "Remote sensing annual dynamics of rapid permafrost thaw disturbances with LandTrendr," *Remote Sens. Environ.*, vol. 268, 2022, Art. no. 112752.

[12] J. Luo, F. Niu, Z. Lin, M. Liu, and G. Yin, "Recent acceleration of thaw slumping in permafrost terrain of Qinghai-Tibet Plateau: An example from the Beiluhe Region," *Geomorphology*, vol. 341, pp. 79–85, 2019.

[13] Z. Xia et al., "Retrogressive thaw slumps along the Qinghai–Tibet engineering corridor: A comprehensive inventory and their distribution characteristics," *Earth Syst. Sci. Data*, vol. 14, no. 9, pp. 3875–3887, 2022.

[14] Q. Zhang, S. Ling, and X. Li, "Comparison of landslide susceptibility mapping rapid assessment models in Jiuzhaigou County, Sichuan province," *China*, vol. 39, no. 8, pp. 1595–1610, 2020.

[15] W. Chen, X. Xie, J. Peng, J. Wang, Z. Duan, and H. Hong, "GIS-based landslide susceptibility modelling: A comparative assessment of kernel logistic regression, Naïve-Bayes tree, and alternating decision tree models," *Geomatics, Natural Hazards Risk*, vol. 8, no. 2, pp. 950–973, 2017.

[16] H. R. Pourghasemi and N. Kerle, "Random forests and evidential belief function-based landslide susceptibility assessment in Western Mazandaran Province, Iran," *Environ. Earth Sci.*, vol. 75, pp. 1–17, 2016.

[17] S. Xu et al., "Landslide susceptibility assessment method incorporating index of entropy based on support vector machine: A case study of Shaanxi Province," *Geomatics Inf. Sci. Wuhan Univ.*, vol. 45, no. 8, pp. 1214–1222, 2020.

[18] D. T. Bui et al., "A novel deep learning neural network approach for predicting flash flood susceptibility: A case study at a high frequency tropical storm area," *Sci. Total Environ.*, vol. 701, 2020, Art. no. 134413.

[19] C. Fei, C. Chao, and L. Xiaoshuang, "Evaluation of landslide susceptibility based on information volume and neural network model," *Chin. J. Rock Mechanics Eng.*, vol. 39, no. 1, pp. 2859–2870, 2020.

[20] J. Goetz, A. Brenning, H. Petschko, and P. Leopold, "Evaluating machine learning and statistical prediction techniques for landslide susceptibility modeling," *Comput. Geosci.*, vol. 81, pp. 1–11, 2015.

[21] F. Huang, Z. Cao, J. Guo, S.-H. Jiang, S. Li, and Z. Guo, "Comparisons of heuristic, general statistical and machine learning models for landslide susceptibility prediction and mapping," *Catena*, vol. 191, 2020, Art. no. 104580.

[22] J. Dou et al., "An integrated artificial neural network model for the landslide susceptibility assessment of Osado Island, Japan," *Natural Hazards*, vol. 78, pp. 1749–1776, 2015.

[23] Q. Zhu, L. Chen, H. Hu, S. Pirasteh, H. Li, and X. Xie, "Unsupervised feature learning to improve transferability of landslide susceptibility representations," *IEEE J. Sel. Topics Appl. Earth Observ. Remote Sens.*, vol. 13, pp. 3917–3930, 2020.

[24] Q. Zhu, M. Zhang, Y. Ding, H. Zeng, W. Wang, and F. Liu, "Fuzzy logic approach for regional landslide susceptibility analysis constrained by spatial characteristics of landslide disaster environmental factors," *Geomatics Inf. Sci. Wuhan Univ.*, vol. 46, no. 10, pp. 1431–1440, 2021.

[25] C. Zhou, K. Yin, Y. Cao, and Y. Li, "Landslide susceptibility assessment by applying the coupling method of radial basis neural network and adaboost: A case study from the Three Gorges Reservoir area," *Earth Sci.*, vol. 45, no. 6, pp. 1865–1876, 2020.

[26] Y. Wang, Z. Fang, R. Niu, and L. Peng, "Landslide susceptibility analysis based on deep learning," *J. Geo-Inf. Sci.*, vol. 23, pp. 2244–2260, 2021.

[27] L. Lv, T. Chen, J. Dou, and A. Plaza, "A hybrid ensemble-based deep-learning framework for landslide susceptibility mapping," *Int. J. Appl. Earth Observ. Geoinf.*, vol. 108, 2022, Art. no. 102713.

[28] Y. Wu, Y. Ke, Z. Chen, S. Liang, H. Zhao, and H. Hong, "Application of alternating decision tree with AdaBoost and bagging ensembles for landslide susceptibility mapping," *Catena*, vol. 187, 2020, Art. no. 104396.

[29] M. Di Napoli et al., "Machine learning ensemble modelling as a tool to improve landslide susceptibility mapping reliability," *Landslides*, vol. 17, no. 8, pp. 1897–1914, 2020.

[30] D. Zou et al., "A new map of permafrost distribution on the Tibetan Plateau," *Cryosphere*, vol. 11, no. 6, pp. 2527–2542, 2017.

[31] J. Błaszczyński and J. Stefanowski, "Actively balanced bagging for imbalanced data," in *Proc. 23rd Int. Symp. Found. Intell. Syst.*, 2017, pp. 271–281.

[32] H. Núñez, L. Gonzalez-Abril, and C. Angulo, "Improving SVM classification on imbalanced datasets by introducing a new bias," *J. Classification*, vol. 34, pp. 427–443, 2017.

[33] S. K. Gupta and D. P. Shukla, "Handling data imbalance in machine learning based landslide susceptibility mapping: A case study of Mandakini River Basin, North-Western Himalayas," *Landslides*, vol. 20, no. 5, pp. 933–949, 2023.

[34] Y. LeCun, Y. Bengio, and G. Hinton, "Deep learning," *Nature*, vol. 521, no. 7553, pp. 436–444, 2015.

[35] Y. He et al., "An extraction method for glacial lakes based on landsat-8 imagery using an improved U-Net network," *IEEE J. Sel. Topics Appl. Earth Observ. Remote Sens.*, vol. 14, pp. 6544–6558, Jun. 2021.

[36] Z. A. Zhao et al., "A comparative study of different neural network models for landslide susceptibility mapping," *Adv. Space Res.*, vol. 70, no. 2, pp. 383–401, 2022.

[37] Y. He et al., "An identification method of potential landslide zones using InSAR data and landslide susceptibility," *Geomatics, Natural Hazards Risk*, vol. 14, no. 1, 2023, Art. no. 2185120.

[38] L.-M. Li, S.-K. Cheng, and Z.-Z. Wen, "Landslide prediction based on improved principal component analysis and mixed kernel function least squares support vector regression model," *J. Mountain Sci.*, vol. 18, no. 8, pp. 2130–2142, 2021.

[39] L. Breiman, "Random forests," *Mach. Learn.*, vol. 45, pp. 5–32, 2001.

[40] E. Goel, E. Abhilasha, E. Goel, and E. Abhilasha, "Random forest: A review," *Int. J. Adv. Res. Comput. Sci. Softw. Eng.*, vol. 7, no. 1, pp. 251–257, 2017.

[41] D. H. Wolpert, "Stacked generalization," *Neural Netw.*, vol. 5, no. 2, pp. 241–259, 1992.

[42] B. Gao et al., "Landslide risk evaluation in Shenzhen based on stacking ensemble learning and InSAR," *IEEE J. Sel. Topics Appl. Earth Observ. Remote Sens.*, vol. 16, pp. 1–18, Jul. 2023.

[43] A. Töscher, M. Jahrer, and R. M. Bell, "The Bigchaos solution to the Netflix grand prize," *Netflix Prize Documentation*, pp. 1–52, 2009.

[44] A. V. Thomas et al., "Landslide susceptibility zonation of Idukki district using GIS in the aftermath of 2018 Kerala floods and landslides: A comparison of AHP and frequency ratio methods," *J. Geovisualization Spatial Anal.*, vol. 5, pp. 1–27, 2021.

[45] H. Chen et al., "A landslide extraction method of channel attention mechanism U-Net network based on Sentinel-2A remote sensing images," *Int. J. Digit. Earth*, vol. 16, no. 1, pp. 552–577, 2023.

[46] A. Arabameri, S. Saha, J. Roy, W. Chen, T. Blaschke, and D. T. Bui, "Landslide susceptibility evaluation and management using different machine learning methods in the Gallicash River Watershed, Iran," *Remote Sens.*, vol. 12, no. 3, pp. 1–29, 2020.

[47] J. F. Hair, "Multivariate data analysis," 2009.

[48] A. Saha and S. Saha, "Comparing the efficiency of weight of evidence, support vector machine and their ensemble approaches in landslide susceptibility modelling: A study on Kurseong region of Darjeeling Himalaya, India," *Remote Sens. Appl., Soc. Environ.*, vol. 19, 2020, Art. no. 100323.

[49] Y. He et al., "A unified network of information considering superimposed landslide factors sequence and pixel spatial neighbourhood for landslide susceptibility mapping," *Int. J. Appl. Earth Observ. Geoinf.*, vol. 104, 2021, Art. no. 102508.

[50] J. R. Mantovani et al., "Novel landslide susceptibility mapping based on multi-criteria decision-making in Ouro Preto, Brazil," *J. Geovisualization Spatial Anal.*, vol. 7, no. 1, pp. 1–17, 2023.

[51] J. Dou et al., "Improved landslide assessment using support vector machine with bagging, boosting, and stacking ensemble machine learning framework in a mountainous watershed, Japan," *Landslides*, vol. 17, pp. 641–658, 2020.
[52] Y. He et al., "An integrated neural network method for landslide susceptibility assessment based on time-series InSAR deformation dynamic features," *Int. J. Digit. Earth*, vol. 17, no. 1, 2024, Art. no. 2295408.
[53] Y. He et al., "Time-series analysis and prediction of surface deformation in the Jinchuan mining area, Gansu Province, by using InSAR and CNN–PhLSTM network," *IEEE J. Sel. Topics Appl. Earth Observ. Remote Sens.*, vol. 15, pp. 6732–6751, Aug. 2022.
[54] S. Yao et al., "A convLSTM neural network model for spatiotemporal prediction of mining area surface deformation based on SBAS-InSAR monitoring data," *IEEE Trans. Geosci. Remote Sens.*, vol. 61, Jan. 2023, Art. no. 5201722.
[55] K. Dai et al., "Entering the era of earth observation-based landslide warning systems: A novel and exciting framework," *IEEE Geosci. Remote Sens. Mag.*, vol. 8, no. 1, pp. 136–153, Mar. 2020.
[56] K. Dai et al., "Interpretation and sensitivity analysis of the InSAR line of sight displacements in landslide measurements," *GISci. Remote Sens.*, vol. 59, no. 1, pp. 1226–1242, 2022.
[57] Y. He, Y. Chen, W. Wang, H. Yan, L. Zhang, and T. Liu, "TS-InSAR analysis for monitoring ground deformation in Lanzhou New District, the loess Plateau of China, from 2017 to 2019," *Adv. Space Res.*, vol. 67, no. 4, pp. 1267–1283, 2021.

Yi He (Member, IEEE) received the B.S. degree in geographic information system from Lanzhou Jiaotong University, Lanzhou, China, in 2011, and the Ph.D. degree in earth system science from Lanzhou University, Lanzhou, China, in 2016.

He has been a Postdoctoral Researcher with the School of Environment and Municipal Engineering, Lanzhou Jiaotong University, Lanzhou, China. He is currently a Professor with the Faculty of Geomatics, Lanzhou Jiaotong University, Lanzhou, China. His research interests include disaster remote sensing, ecological remote sensing, image processing and time series InSAR prediction based on deep learning.

Tianbao Huo received the B.E. degree in surveying and mapping engineering in 2022 from the Lanzhou Jiaotong University, Lanzhou, China, where he is currently working toward the M.S. degree in mapping science and technology with the Faculty of Geomatics.

His research interests include land subsidence monitoring and time series InSAR prediction based on neural networks.

Binghai Gao received the B.E. degree in remote sensing science and technology in 2021 from the Lanzhou Jiaotong University, Lanzhou, China, where he is currently working toward the M.S. degree in mapping engineering with the Faculty of Geomatics.

His research interests include InSAR data processing technology, deep learning, and remote sensing image information extraction.

Qing Zhu received the B.S. and M.S. degrees in aerial photogrammetry from Southwest University, Chongqing, China, in 1986 and 1989, respectively, and the Ph.D. degree in railway engineering from North Jiaotong University, Beijing, China, in 1995.

In 1997, he was a Professor with the State Key Laboratory of Information Engineering, Surveying, Mapping and Remote Sensing, Wuhan University, Wuhan, China. Since 2014, he has been a Professor and the Director of Research Committee with the Faculty of Geosciences and Environmental Engineering, Southwest Jiaotong University, Chengdu, China. He is currently a Visiting Professor with the Wuhan University, Wuhan, China, Central South University, Changsha, China, and Chongqing University, Chongqing, China. He has authored or coauthored more than 260 articles and 7 books. His research interests include photogrammetry, geographic information system, and virtual geographic environment.

Dr. Zhu was the recipient of the Cheung Kong Scholars in 2009.

Long Jin received the B.E. degree in remote sensing science and technology in 2023 from the Lanzhou Jiaotong University, Lanzhou, China, where he is currently working toward the M.S. degree in resources and environmental engineering with the Faculty of Geomatics.

His research interests include 3-D deformation monitoring for mining areas and phase unwrapping.

Jian Chen received the B.E. degree in surveying and mapping engineering from Southwest Jiaotong University, Chendu, China, in 2021. He is currently working toward the M.S. degree in mapping science and technology with the Faculty of Geomatics, Lanzhou Jiaotong University, Lanzhou, China.

His research interests include retrogressive thaw slumps detection and extraction based on deep learning combined with remote sensing data.

Qing Zhang received the B.E. degree in surveying and mapping engineering in 2022 from the Lanzhou Jiaotong University, Lanzhou, China, where he is currently working toward the M.S. degree in mapping science and technology with the Faculty of Geomatics.

His research interests include InSAR data processing technology, machine learning, and remote sensing image processing.

Jiapeng Tang received the B.E. degree in remote sensing science and technology in 2021 from Lanzhou Jiaotong University, Lanzhou, China, where he is currently working toward the M.S. degree in mapping science and technology with the Faculty of Geomatics.

His research interests include InSAR data processing technology, and geological hazard identification of highway corridor in loess area.